MODELLING OF THERMOMECHANICAL ROLLING

E.J. Palmiere[†], C.M. Sellars[†] and S.V. Subramanian[‡]

[†]Institute for Microstructural and Mechanical Process Engineering:
The University of Sheffield, Department of Engineering Materials,
Sir Robert Hadfield Building, Mappin Street, Sheffield S1 3JD, UK

[‡]Department of Materials Science and Engineering, McMaster University
1280 Main Street West, Hamilton, Ontario L8S 4M1, Canada

Abstract

Over the past 20 years following on from the international conference Niobium 81, considerable progress has been made regarding the development of mathematical models for thermomechanical rolling, from the point of solidification through to the end of finish rolling. As one would expect, certain areas have received far more attention, and are consequently more developed, than other areas. The present paper reviews the key elements associated with those areas which have been reasonably "well-developed", and highlights other areas where understanding is only semi-quantitative at best. Hence, in addition to offering a review of the relevant work from the past 20 years, the paper is very much intended to provide a look forward to those critical components necessary for the establishment of a complete and quantitative "through-process", physically-based model for the rolling of microalloyed steels.

Introduction

At the time of the previous Niobium conference in 1981, the mathematical modelling of thermomechanical processing, particularly with regard to the incorporation of microstructural evolution into the models, was in its infancy. Although there was a substantial body of knowledge about the physical metallurgy of microalloyed steels (1), the methodology for quantifying the effects on recrystallization and grain size evolution of austenite during multipass rolling had only just been developed (2,3). It is now widely recognized that some microstructural parameters (S) must be included within the models of thermomechanical processing, as indicated in Figure 1 (4), because of their effects on flow stress (σ) during hot working and on the subsequent phase transformation on cooling, and hence on product properties. The sensitivity of the microstructural evolution to the external variables of strain (ε), strain rate ($\dot{\varepsilon}$), temperature (T) and time (t) requires inputs to the microstructural model from the deformation and temperature models to define the local conditions throughout the processing operations. Today, the advances in computing power and the developments of 2D and 3D thermomechanically coupled finite element modelling packages have removed any limitations from the detail with which the local conditions can be computed, except from the viewpoint of the accuracy with which the boundary conditions of heat transfer and friction are known. These are the subject of active research to develop a soundly based physical model for the behavior of secondary and tertiary scale during rolling (5), as this governs the boundary conditions, however this aspect of modelling thermomechanical rolling of microalloyed steels will not be considered further in this paper.

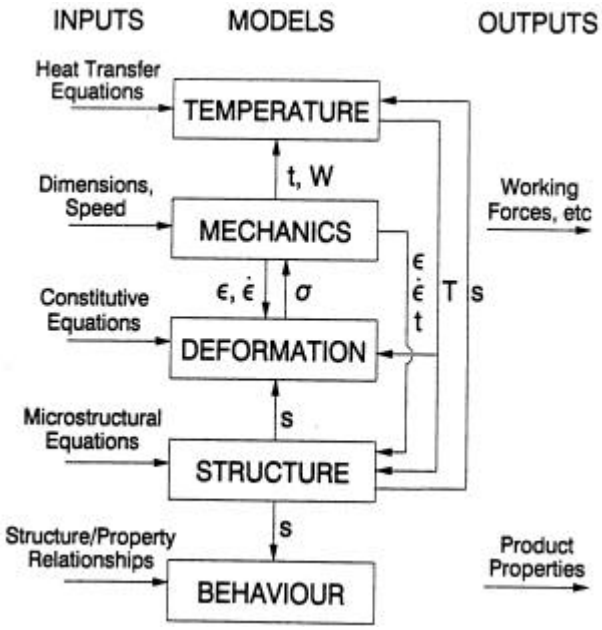

Figure 1: Schematic diagram of the components of models for industrial hot forming processes (s=structure, t=time, T=temperature, W=work, ε=strain, $\dot{\varepsilon}$=strain rate, σ=stress) (4).

The commercial value of having sound models to both optimise and control the conditions of thermomechanical rolling, rather than relying on the traditional trial-and-error methods, is now driving further developments of modelling to encompass the full process history from liquid steel to finished product properties (such as strength, toughness and formability) and attributes (such as surface quality) within a coherent "through-process" model (6).

The focus of the present paper is, however, to consider only the current state-of-the-art, as far as the microstructural evolution in niobium microalloyed steels is concerned, with the constraints on length of the paper limiting this to the austenitic condition and to the end of rolling. The basis of all models is in the accurate representation of the equilibrium state from thermodynamics and to use this to predict the kinetics of dissolution and reprecipitation under the non-equilibrium conditions of industrial processing. A complete model of the rolling stage of thermomechanical processing should, in addition to microstructure, provide an input to the transformation model on residual solute content and its distribution in the matrix. Because microstructure cannot be observed directly under rolling conditions, the microstructural consequences on flow stress should also be modelled. Such changes in flow stress have been widely used in laboratories to quantify the microstructural effects, and the load data routinely gathered in modern mills can be used in similar ways to validate model outputs and to improve accuracy with the limited range of variables in a specific mill.

Thermodynamic Modelling to Predict Mole Fraction, Composition and Phase Separation of Precipitates in Microalloyed Steels

Thermodynamic Analysis of Precipitation of Interstitial Compounds in Austenite

Thermodynamic analysis is essential for the quantitative modelling of the kinetics of precipitation during the thermomechanical processing of microalloyed steel. The industrial alloys invariably contain more than one microalloying element, which influence the thermodynamics of the precipitation behaviour. The occurrence of carbonitride precipitates in austenite and the mutual solubility of the carbides and nitrides of microalloying elements in the precipitates is well established (7). The most common approach used in analysing the experimental data on carbonitride precipitation in austenite has been to adopt the Hillert-Staffanson model (8). This model assumes that the metal atoms M(Niobium, Titanium, Vanadium) and interstitial atoms X(Carbon, Nitrogen) mix randomly on the two sub-lattices of the rock salt structure of the interstitial MX compound. The free energy of the precipitate is described by a regular or sub-regular solution model, which requires detailed knowledge of the relevant thermodynamic data. Chemical potentials of solutes in austenite are described assuming dilute solution behaviour of the regular or sub-regular solution model depending upon the concentration of the elements present. The lack of availability of reliable thermodynamic data on interaction energy has led to simplifying assumptions until recently. The effect of ignoring the interaction energy results in ideal solution behaviour. The early approach by Irving, Pickering and Gladman (9) was to combine the carbon and nitrogen effect in the pseudo-binary solubility product to describe the precipitation of Nb(C,N), which approximates to an ideal solution behaviour. However, the validity of such an approach is restricted to the domain of experimental databases. With the availability of more experimental data on interaction energy, comprehensive models with predictive capability have been developed that include thermodynamic interaction energy. However, the models differ in the treatment of excess free energy that deals with thermodynamic interactions.

Ohtani et al. (10) have analysed the thermodynamics of the Fe-Nb-C system using a regular solution model to deal with a concentrated solution of carbon. The strong interaction between niobium and carbon atoms in austenite leads to marked reduction in the chemical potential of niobium in a high carbon region. In consequence, the solubility curve for NbC is described by Equation 1, which contains an additional term for the concentration dependence on carbon.

$$\log([\%Nb][\%C]) = -\frac{4880}{T} + 1.18 + [\%C](\frac{1590}{T} - 0.1) \quad (1)$$

Thus, the effect of raising the carbon content is to increase the solubility product of NbC. This has the net effect of retaining more niobium in solution in a high carbon compared with in a low carbon austenite matrix. The solubility product of NbC is influenced by chemical interactions with other solutes present in the multi-component system. For example, the strong interaction between manganese and carbon in austenite decreases the activity of carbon, which has the net effect of increasing the equilibrium solubility product of NbC. Koyama et al. (11) have investigated the effect of manganese on the solubility product of NbC in austenite, which is described by the following expression:

$$\log([\%Nb][\%C]) = -\frac{7970}{T} + 3.31 + (\frac{1371}{T} - 0.9)[\%Mn] - (\frac{75}{T} - 0.0504)[\%Mn]^2 \quad (2)$$

Akben, Weiss and Jonas (12) attribute the retardation of the dynamic precipitation of NbC in austenite in high manganese steel in part to the increased solubility product of NbC shown in Equation 2. Thermodynamic analysis predicts that NbC precipitates will deviate from stoichiometry because of equilibrium vacancy concentration, which will increase with temperature. The effect of non-stoichiometry, and chemical interaction on the solubility product of NbC in austenite can be quantitatively analysed as a function of temperature (13). It should be noted that the strong chemical interaction between carbon and niobium is beneficial in suppressing the NbC eutectic formation in the interdendritically microsegregated liquid during the dendritic solidification of medium carbon niobium microalloyed steels (14).

Regular Solution Model for Predicting the Carbonitride Precipitation

Quantitative modelling based on Hillert and Staffanson's regular solution model is used for predicting the equilibrium mole fraction and the microchemistry of the precipitates of the compound (Ti_xNb_{1-x}) (C_yN_{1-y}) as a function of base chemistry and temperature. Nishizawa (15) has reviewed the thermodynamics of phase equilibria relating to carbonitride precipitation in microalloyed steels using a regular solution model. Akamatsu et al. (16) have used a regular solution model using Thermocalc to predict phase stability of carbonitride precipitates in an interstitial free steel microalloyed with niobium and titanium. Inoue et al. (17) have used a sub-regular solution model to predict of the phase equilibria between austenite and (Nb,Ti,V) (C,N) precipitates in microalloyed steels. The basic work on phase separation of interstitial compounds by Rudy (18) has been extended in the modelling work of Inoue et al. (17) to predict the phase separation events occurring in complex microalloyed precipitates. Thus the capability to model the thermodynamics of complex microalloying systems has advanced significantly in recent years to predict phase separation in complex precipitates. The validations of the modelling and some salient features of the recent advances in modelling, including phase separation, are examined briefly.

The experimental approach to validate the model is based on TEM/STEM experimental results on precipitate microchemistry of equilibrated samples and precipitate dissolution temperature studies. The models are used with reasonable success to interpret the results on the precipitation studies of microalloyed steels, but the precision with which the interstitial concentration of carbonitride precipitates can be determined does not allow for the rigorous validation of the non-stoichiometry of the precipitates. In modelling the carbonitride precipitation in a niobium-titanium microalloyed steel, Grujicic et al. (19) have considered the variation in the equilibrium compositions of austenite and precipitation over a range of

temperatures. The Kohler temperature–dependent sub-regular solution model is used to describe the austenite phase. The (Nb,Ti) (C,N) precipitate phase is described by the Hillert-Staffanson sub-lattice model for a four component system with components mixed in pairs. The equilibrium between the two phases is explored while allowing for the non-stoichiometry of the precipitate phase. The results are shown to be in good agreement with experimental data on ultra-low carbon steels microalloyed with niobium and titanium.

Zou and Kirkaldy (20) have extended the regular solution model to include the surface energy term in order to treat the kinetics of the early stages of precipitate growth, when the capillarity effect is expected to be significant because of the small radius of curvature of the precipitates. The validity of the model was tested in their work on precipitation in the Fe-Nb-Ti-C-N system, but experimental limitations did not allow for a rigorous validation of the model.

Thermodynamic Modelling of Phase Separation in Mixed Carbonitrides

Figure 2 is a schematic illustration of phase separation in a Nb-Ti-C-N system after Nishizawa (15). The apexes at the four corners are pure compounds of NbC, TiC, TiN and NbN respectively. The coordinating axes represent the site fractions of titanium and nitrogen respectively as indicated on the schematic. The ordinates represent the Gibbs free energy. In the centre of the diagram, the miscibility gap is predicted from the tie-line sets between TiN-like and NbC-like phases. These are predicted to be stable below the critical temperature. The miscibility gap is caused by the difference in chemical stabilities of the pure compounds, TiN being more stable than the rest as indicated by the lowest Gibbs free energy. The miscibility gap is represented by the binodal curve, and is caused by the decomposition reactions to form the stable TiN-like and NbC-like phases (NbN + TiC = TiN + NbC). This schematic illustrates the surface of integral free energy of mixing at a fixed temperature, which is well below the critical temperature for phase separation. It should be noted that the critical temperature for the phase separation of (Nb,Ti) (C,N) is high (2177ºC) compared with (Nb,V) (C,N) (976ºC) and (Ti,V) (C,N) (1174ºC) systems. Below the critical temperature, phase separation is predicted. Thus, there is clearly a thermodynamic potential for phase separation in Nb-Ti carbonitride precipitates even at high temperatures, which has to be considered when modelling such systems. There is potential for spinoidal decomposition within the miscibility gap, which is predicted to give stable phase separation without the nucleation barrier. Just outside the spinoidal decomposition regime, the separation of metastable phases involves nucleation and growth steps. The modelling capability is advanced to predict binodal and spinoidal curves for complex carbonitride precipitates as a function of temperature.

Quantitative modelling of the phase equilibria between austenite and (Nb,Ti,V) (C,N) predicts that the effect of adding vanadium to a Nb-Ti system is to promote phase separation of TiN and NbC phases, but VN will remain dissolved in the TiN phase. On the other hand, if niobium is added to a Ti-V system, the VC phase is replaced by the NbC-rich phase. In consequence, the phase separation of the TiN and NbC-rich phase occurs but VC will remain dissolved in the NbC phase. If titanium is added to a Nb-V system, VN is replaced by a TiN-rich phase. Thus, the modelling allows the prediction of the temperature effect on the phase separation of carbonitrides as well as the composition of the phases. Grain growth stability of phases located within the spinoidal regime of the carbonitride system presents a technological opportunity for precipitate size and dispersion control, which has yet to be exploited in microalloyed steels.

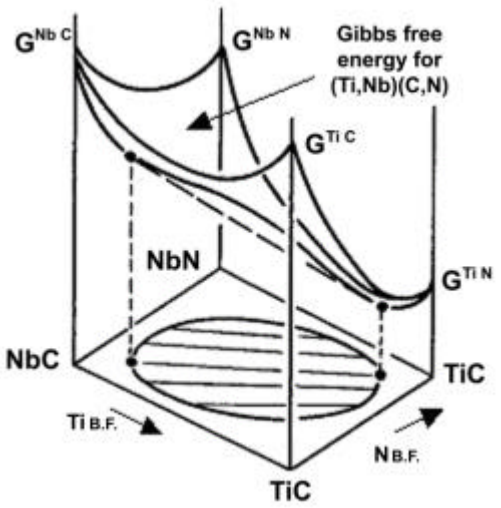

Figure 2: A schematic representation of the miscibility gap in the Gibbs free energy diagram for a Nb-Ti carbonitride at a constant temperature showing the tie line for the phase separation of NbC-rich and TiN-rich phases respectively. Both $Ti_{S.F.}$ and $N_{S.F.}$ are the site fractions of titanium and nitrogen respectively (15).

Studies on the precipitation behaviour of a medium carbon steel microalloyed with titanium and vanadium showed that metastable dendritic precipitates of mixed nitrides of titanium and vanadium occur in the as-cast bloom. Upon homogenisation at 1100ºC, long dendritic precipitates of (Ti,V)N were found to fragment, resulting in an array of fine precipitates enriched in TiN. Phase separation is not expected in (Ti,V)N at 1100ºC. However, phase separation is predicted at a temperature below 1174ºC if a carbonitride is assumed. The experimental technique did not permit the determination of the carbonitride composition with precision to validate the model prediction (21). Further studies are required to validate the model predictions on phase separation in microalloyed steels of technological interest.

Quantitative Modelling of the Solidification Behaviour of Microalloyed Steels

Modelling of Solute Redistribution Due to Dendritic Solidification

The precipitation behaviour of microalloyed steel is influenced by solute redistribution from dendritic solidification of steel in the caster and the post-solidification cooling schedule. The current trend is to integrate the rolling with the casting process. The objective is to avoid the energy intensive reheating process by rolling the slab directly while it is hot (i.e., hot direct rolling) or charge the slab while it is hot in order to conserve the sensible heat (i.e., hot charge process). The energy consumption of slab cold charging is 1400 KJ/kg, which can be decreased to 200 KJ/kg by direct rolling the slab at 1150ºC or 750 KJ/kg by hot charging the slab at 650ºC. The starting structure for hot direct rolling is that inherited from the as-cast state, which exhibits chemical inhomogeneity due to microsegregation. Therefore, it is important to understand the influence of the base chemistry, solidification processing and post-solidification cooling schedule of the slab in the caster on the precipitation behaviour of microalloying elements during thermomechanical processing. The solidification structure is expected to play a dominant role on the precipitate evolution of microalloyed steels in near-net shape processing, such as strip casting. The early impetus for solidification modelling of steels microalloyed with niobium in the caster arose because of surface cracking during bending and straightening of the slab in the caster. This was traced to the broadening of the ductility trough caused by niobium carbonitride precipitation. Coarse precipitates of NbC occurred at the grain

boundaries causing the solute denuded zone, coupled with dynamic strain-induced precipitation of fine NbC occurring within the matrix because of deformation at a low $\dot{\varepsilon}$ (10^{-4} sec^{-1}), contributed to strain localisation at the grain boundaries. The intergranular fracture was caused by the occurrence of microvoid coalescence (22-24).

Dendritic solidification of the steel causes a concentration variation on a local scale, which is of the order of the interdendritic spacing. The interdendritric spacing ranges typically from 30-1000 μm, depending on the local solidification rates occurring in industrial slabs. During the solidification of steels, the dendrite spacing is empirically related to the local solidification time (the resident time between the liquidus and solidus) raised to the power of an exponent that ranges from 0.5 to 0.33. The faster the cooling rate, the finer the interdendritic spacing. If the steady state dendritic solidification is disturbed by fluid flow, the solute enriched liquid may be transported over a large distance, resulting in macrosegregation. While macrosegregation can be prevented by the control of fluid flow in the caster, microsegregation is inherent in the mechanism of dendritic solidification.

A quantitative model has been developed to predict the solute redistribution from dendritic solidification for multicomponent microalloyed steels (25). A finite difference method is used to predict the microsegregation at a given location (node point) in the slab. The diffusion equation is represented by the Crank-Nicholson implicit method of a finite difference equation. Local equilibrium is assumed at the solid–liquid interface.

Multi-component phase equilibria are rigorously calculated from thermodynamic data for the case of Fe-Mn-C because of the large Mn concentration in the steel. The effects of other alloying elements are taken into account as a first order correction to this base. The slab thermal history used in the analysis is typical of an industrial caster. The algorithm results in the computation of the interdendritic microsegregation during freezing (including the effects of solid state diffusion during freezing) at stage-I and modifies this result by accounting for post-solidification homogenization in the δ-ferrite (stage-II), in the δ+γ field (stage-III) and in the single phase γ region (stage-IV), shown in Figure 3. Quantitative results of microsegregation in a typical high niobium, titanium bearing line pipe steel (0.03% carbon, 0.003% nitrogen, 0.09% niobium, 0.014% titanium solidifying at a location 5mm from the slab surface with an interdendritic spacing of 70μm are analyzed for the typical cooling schedule of the industrial caster.

The solute redistribution of carbon and nitrogen exhibits a negligible variation in the concentration in the solid as a function of fraction solidified. The interstitial solutes exhibit negligible microsegrgation, suggesting that the diffusion of the interstitial solutes is able to keep pace with the rate of advance of the solid-liquid interface during solidification. In contrast, the substitutional solutes give rise to significant microsegregation that persists to lower temperatures. Figures 4 and 5 show the redistribution of solute niobium and titanium respectively as a function of distance from the centre of a dendrite arm. The reduction in the intensity of microsegregation as defined by carbon maximum/carbon minimum from Stage-I to Stage-II, corresponding to the δ phase field (BCC structure), is far more significant than those of stage-III and stage-IV, because the diffusion coefficients of niobium and titanium in the δ phase are about 100 times greater than those in the γ phase (FCC structure). An increase in the temperature window of the δ phase field, corresponding to a decrease in the carbon content, brings about a significant homogenisation of the substitutional solutes. By comparison, the degree of homogenisation is not significant in austenite at a lower but wider temperature range corresponding to stage-IV.

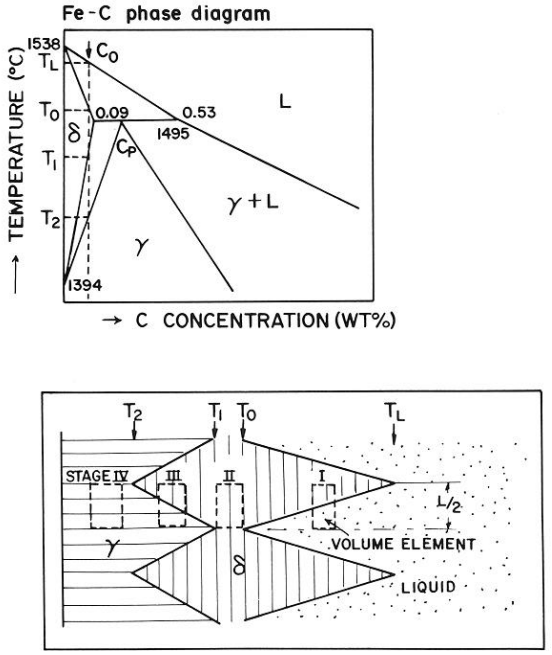

Figure 3: A schematic diagram representing the various stages of microsegregation during solidification (Stage I) and post-solidification homogenisation (Stages II, III and IV) (25).

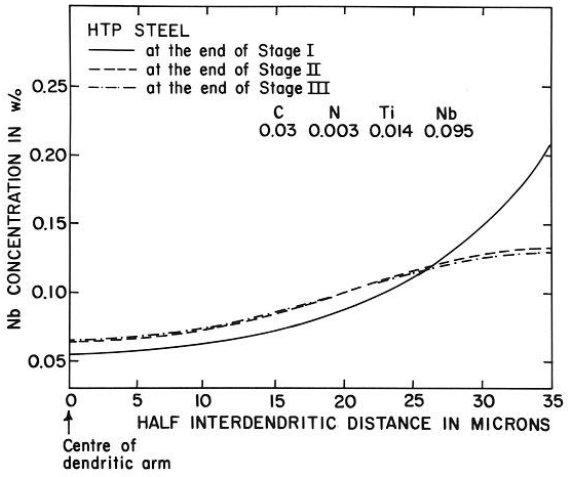

Figure 4: The distribution of niobium as a function of interdendritic distance at the end of Stage I, II and III respectively (25).

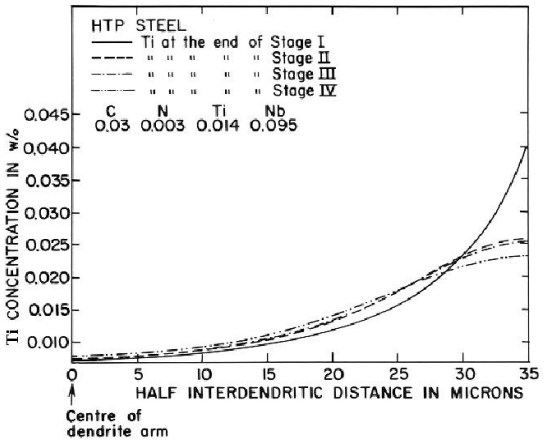

Figure 5: The distribution of titanium as a function of interdendritic distance at the end of Stage I, II, III and IV (1200ºC) respectively (25).

The effect of decreasing the carbon content in a given base chemistry was found to decrease the degree of microsegregation of niobium and titanium. The effect of lowering carbon is to increase the temperature window in the δ phase field, where significant diffusional homogenisation of substitutional solute occurs. Thus, a distinct advantage of low carbon design is to reduce the intensity of the microsegregation of the substitutional solutes, thereby promoting a more homogeneous microstructure. The reduced tendency of microsegregation in microalloyed steels with low carbon has been reported by Taira et al. (26) using mill data, which is consistent with the foregoing analysis.

The microsegregation and precipitation models are used to design the base chemistry and temperature window required to prevent surface cracking during the bending and straightening

of the slab. The base chemistry is designed to reduce the intensity of microsegregation using a low interstitial design. Titanium additions are made to the stoichiometric requirement to tie up all the nitrogen at high temperatures as TiN. This is possible only if the nitrogen content of the steel is controlled to low levels (<40 ppm). A low carbon design ensures less intensity of microsegregation of niobium, which allows an adequate niobium addition so that the thermodynamic potential for precipitation of NbC is only reached at a temperature well below the temperature window of bending and straightening of the slab. Thus, quantitative analysis of both the solidification and precipitation behaviour of a titanium-niobium microalloyed steel has underscored the scientific merits of low nitrogen as well as low carbon design in order to obtain sound slabs without surface cracking, which can be thermomechanically processed to impart strength.

Precipitate Evolution in Slabs

The morphology and microchemistry of the precipitates occurring in the slabs have been characterised using Transmission Electron Microscope (TEM/STEM) techniques. The precipitate morphologies comprised coarse dendritic precipitates, cubic, angular and spiked precipitates. Figure 6 shows a bright field TEM extraction replica of a typical dendritic precipitate of (Nb,Ti) (CN) occurring in the interdendritic region in association with a MnS inclusion. On reheating and holding each steel at a temperature just above the temperature for mixed carbide or carbonitride precipitation, only cuboidal nitride precipitates were found to be stable, as shown in Figure 7. The $C_{Ti}/(C_{Ti}+C_{Nb})$ ratio is smaller in dendritic precipitates than in cubic, angular and spiked precipitates, suggesting that the evolution of dendritic growth of niobium-rich carbides occurs at a lower temperature. These observations suggest that growth of the NbC-rich phase occurs on pre-existing TiN-rich particles. The implication is that if TiN particles are well dispersed, growth of NbC will occur preferentially on the pre-existing particles rather than nucleating independently. This has been confirmed by experimental investigations on flow stress measurements during the hot torsion of a low interstitial steel. The temperature corresponding to the flow stress increase is 1060ºC, which coincides with the equilibrium temperature of precipitation of the Nb-rich mixed carbides (27).

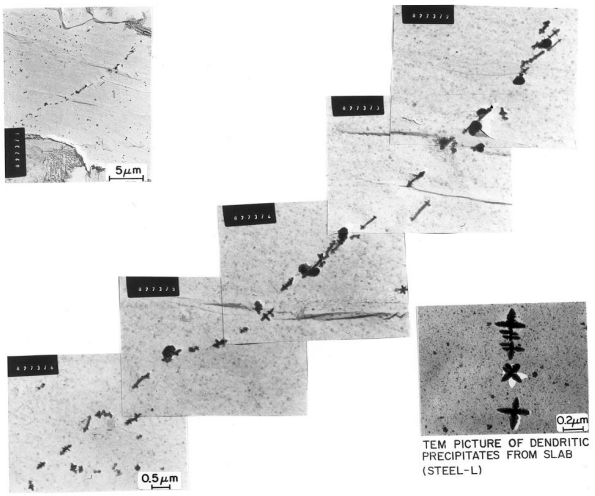

Figure 6: TEM micrograph of an extracted aluminium replica showing the dendritic precipitates occurring along with MnS inclusions in the interdendritically segregated region (27).

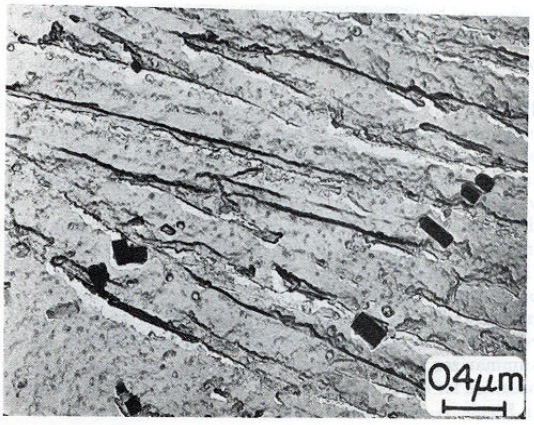

Figure 7: Dendritic precipitates dissolve on holding at 1160ºC, giving cuboidal precipitates of TiN (29).

The recrystallization-limit temperature (RLT), discussed later in the paper, which is based on the strain-induced precipitation of NbC interacting with recrystallization as predicted from the model of Dutta and Sellars, is 936ºC (28). TEM examination of precipitates interrupted during hot torsion simulation by quenching shows that the inner core of the precipitate is enriched in TiN upon which niobium enriched carbides have grown. The increase in flow stress is attributed to the increase in the Zener drag force on the boundary mobility caused by the epitaxial growth of NbC on pre-existing TiN particles. This obviates the need for the strain-induced precipitation of NbC isolated from TiN. However, it is essential to obtain a good dispersion of TiN precipitates in the austenite in the first place, in order to ensure the epitaxial growth of the carbides. To obtain a uniform dispersion of TiN, the microsegregation of titanium in the austenite has to be minimised so that the degree of supersaturation for the precipitation of TiN is homogeneous and the precipitation of TiN should be promoted in austenite (29). Most mill operators regard the up-stream process controls required to obtain a consistently fine dispersion of TiN as special and exacting. Therefore, the approach is to use the strain-induced precipitation of NbC as the basis for obtaining a uniform dispersion of second phase particles to retard the static softening kinetics.

Modelling Growth of Precipitates and Residual Nb Content as a Function of Cooling Schedules

Assuming a uniform dispersion of TiN precipitates, the growth of NbC on the TiN particles can be represented by the Wagner-Seitz array of equi-sized and equi-spaced spherical particles, enveloped by diffusion fields as shown schematically in Figure 8a. An idealised size (10nm in diameter) and a uniform distribution (300nm interparticle spacing) are assumed at the start. The model for the diffusion-controlled growth of NbC in austenite involves the simultaneous solution of a set of diffusional, equilibrium and mass balance equations (30). These equations are nonlinear and transcendental in nature, requiring iterative methods for solution. The mole fraction of the precipitates, the particle diameter and the residual niobium content of the matrix are calculated for cooling rates, from 0.5 to 10°C/s, commencing from the equilibrium temperature for the precipitation of NbC. The growth of the precipitates occurs predominantly in the higher temperature region (>850°C). The time for diffusional growth is determined by the cooling rate. The residual niobium is plotted as a function of cooling rates, as shown in Figure 8b. The model based on volume diffusion shows that the matrix will be depleted of niobium only at slow cooling rates. As discussed later, volume diffusion is essential for an increase in the volume fraction of precipitates, although enhanced diffusion along dislocations and grain boundaries provides some acceleration.

Diffusional Homogenisation of Microsegregation

The diffusion coefficients of niobium and titanium in austenite are very low and are of similar order to that of the self-diffusion of iron. Significant homogenisation of the substitutional solutes niobium and titanium is possible at reasonable temperatures and times only if the material has fine dendrite spacings (<50 μm), which are only obtained at less than 5 mm from the surface of a thick slab as a result of rapid solidification (31,32). For a typical dendrite spacing of 300 μm, for significant though not complete homogenisation to occur, the ingot has to be held at 1175ºC for 20 hours. The residual segregation index, $d = (C^h max. - C^h min.)/(C^i max. - C^i min.)$, where i and h stand for the initial and homogenised condition respectively, is decreased only to 0.2 even after such a long homogenisation treatment. If the dendrite spacing is much larger, homogenisation is more difficult to achieve. Thus, in the slowly cooled regions of the slab where the interdendritic spacing tends to be large, it is difficult to anneal out the chemical inhomogeneity caused by microsegregation. This

concentration variation caused by the microsegregation of microalloying elements will therefore persist and continue to influence the precipitate evolution during downstream processing. Hence, any modelling on precipitation should consider the residual segregation index of microalloying elements.

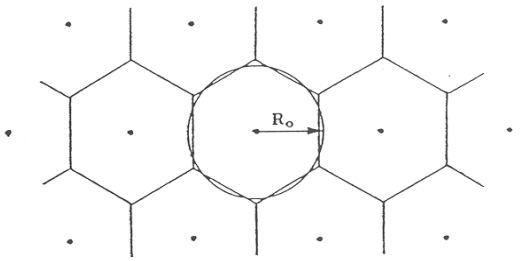

Figure 8a: Schematic of a Wagner-Seitz array of equi-sized and equi-spaced particles enveloped by diffusion fields. NbC is assumed to grow epitaxially on TiN particles of 10 nm diameter, uniformly dispersed with an interparticle spacing of 300 nm (30).

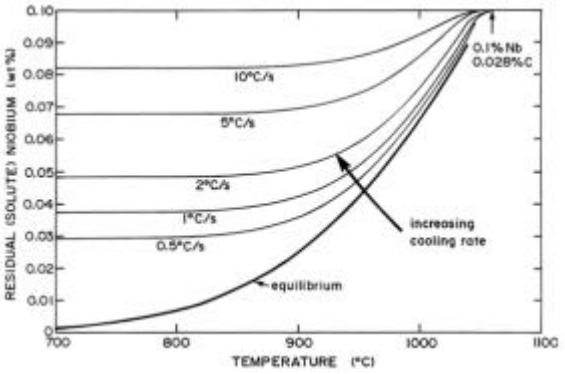

Figure 8b: Residual (solute) Nb plotted as a function of temperature for various cooling rates. Model assumes ideal size and dispersion of particles and growth by volume diffusion in the matrix (30).

Modelling the Kinetics of Strain-Induced Nb(CN) Precipitation During Hot Rolling

The precipitation of microalloying elements such as niobium play a major role in controlling the final microstructure and hence the properties of steel products. The pinning force exerted by fine precipitates on subgrain boundaries suppresses the process of recrystallization, thus enabling the retention of the deformed austenite structure from one rolling pass to the next. As a result of particles inhibiting recrystallization, which subsequently leads to a higher recrystallization-stop temperature, controlled rolling practice can occur at higher temperatures and at smaller rolling loads (28,33-37). Besides increasing the recrystallization-stop temperature, the presence of precipitates also increase the grain coarsening temperature (38), which plays an important role during controlled reheating practices. Considering the enormous practical significance of the precipitation process, it is essential to understand the mechanisms of precipitation during the hot rolling of microalloyed steels.

A large number of researchers have studied the precipitation kinetics of these microalloying elements and their subsequent effect on the microstructure. Results of these studies conclusively show that prior deformation enhances the precipitation kinetics significantly (1,28). Incidentally, these studies involve a number of variables such as steel composition, initial grain size, deformation temperature, amount of strain, strain rate and type of deformation etc. In addition, these studies also employ a variety of techniques for precipitate detection, and size and volume fraction measurements. As a result, it is difficult to make a direct comparison of all the experimental results. Initially, Dutta and Sellars (28) proposed a model to predict the precipitation start (corresponding to 5% precipitation) time for noibium microalloyed steels. This model was based on an extensive analysis of available experimental results and classical nucleation theory. An essential feature of this model was that, by combining semi-empirical equations for the start of static recrystallization with the precipitation kinetics model, it shows a high temperature regime where complete recrystallization takes place, and an intermediate

temperature regime between the end of recrystallization (i.e., before the start of precipitation and defined as the recrystallization-limit temperature, RLT, or $T_{95\%}$) and the start of precipitation before recrystallization (i.e., defined as the recrystallization-stop temperature, RST, T_{nr} or $T_{5\%}$), below which no recrystallization occurs, as shown in Figure 9 (37). Although this model was simple and showed reasonably good agreement with many of the experimental data, it did not consider the complete precipitation kinetics, i.e. the evolution of precipitate volume fraction and size with time. A similar model was proposed for titanium microalloyed steels (34). This work was followed up by a detailed model by Liu on niobium-steels (39).

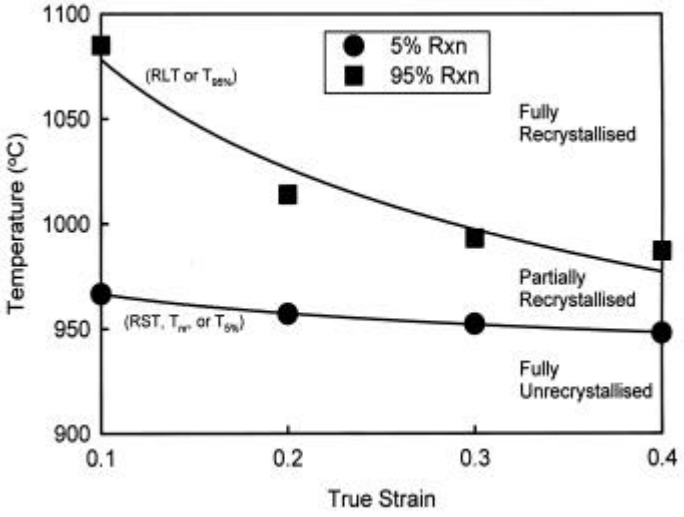

Figure 9: Effect of prestrain on the recrystallization-stop temperature (RST, T_{nr} or $T_{5\%}$ - corresponding to 5% RXN) and the recrystallization-limit temperature (RLT or $T_{95\%}$ - corresponding to 95% RXN). Steel consisted of 0.1C-0.03Nb-0.005N and was initially reheated to 1250°C. Deformation took place at $\dot{\varepsilon}=10$ sec^{-1} and the interpass delay time was 10 seconds (37).

Although this model considered the heterogeneous nucleation of precipitates on dislocations and enhanced growth due to pipe diffusion through dislocations, it did not consider the concurrent precipitate coarsening process. This was in contradiction to the observations of Dutta et al. (35) who had shown that the coarsening began at a very early stage of precipitation and subsequently led to a significant decrease in precipitate number density. Interestingly, Dutta et al. (35) also showed that the growth and coarsening occur simultaneously during the precipitation. However, until the development of the recent model (40), comprehensive consideration of the precipitation kinetics describing the nucleation, growth and coarsening of precipitates was lacking in the literature.

Earlier work has shown that the presence of dislocations caused a significant acceleration in the nucleation, growth and coarsening of precipitates (28,34-42). The early occurrence of coarsening is assumed to be an essential feature in strain-induced precipitation (35). This is illustrated through a schematic diagram in Figure 10 showing an array of precipitates, which initially were situated on dislocation nodes (represented by the solid lines) following one deformation pass. Assuming that the matrix concentration at the precipitate/matrix interface is the equilibrium concentration at the respective deformation temperature, and the concentration in the solute depleted zone around the precipitates is around 95% of that of the bulk concentration, the size of the solute depleted zone is given by $R_{sol}=18R$ (where R is the precipitate radius) when the solute diffusion is controlled by volume diffusion, Figure 10a. It should be noted that the precipitate distribution is assumed to be bimodal in this representation where half of the precipitates are of 1nm radius while the other half are of 1.5 nm radius.

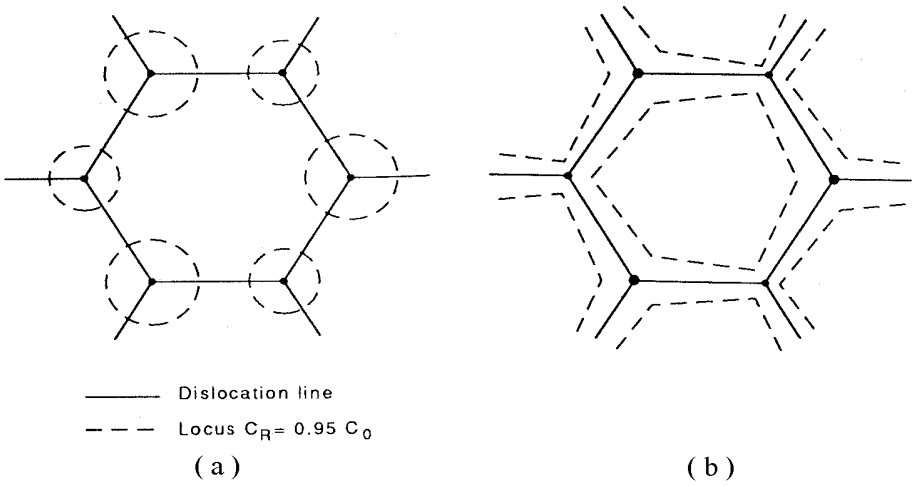

Figure 10: Schematic illustration showing the presence of precipitates on dislocation nodes and solute diffusion fields surrounding the precipitates when: (a) diffusion is due only to volume diffusion and (b) solute diffusion takes place along dislocations. Solid lines represent dislocations and dashed lines indicate the limits of the solute depleted regions (35).

The notable feature of Figure 10a is that the solute depleted zones around the precipitates do not overlap with each other, which in turn implies that the coarsening of precipitates, leading to the growth of bigger precipitates at the expanse of smaller precipitates, cannot occur if the diffusion is dominated by volume diffusion. However, experimental observations after single-pass deformation indicate that further annealing leads to the coarsening of precipitates with a decrease in the precipitate number density (35). It is also observed that an increase in precipitate volume fraction takes place simultaneously with coarsening. All these observations together indicate that bulk diffusion is not the dominant mechanism, and that coarsening begins at a very early stage during strain-induced precipitation. These observations can only be explained by considering the effect of accelerated solute diffusion along the dislocations, whereby, coarsening can easily occur since the precipitates are interconnected through the dislocation network, Figure 10b. It has been shown (35) that this assumption leads to a reasonable estimate of the precipitate size evolution kinetics. This paper summarizes the key features of a model to predict the complete precipitation kinetics during the strain-induced precipitation in steels microalloyed with niobium.

The present model is based on classical nucleation theory (43-45), and incorporates the changes influenced by the presence of dislocations. It is assumed that the precipitates nucleate heterogeneously on dislocation nodes. This has been proved to be a reasonable assumption based on a previous investigation (35). As discussed before, the effect of dislocations on the diffusion of solutes has been taken into account during the growth and coarsening of the precipitates. The major advantage of the present model is that it provides a complete description of the volume fraction and size evolution of the precipitates, and hence, it can be coupled with the recrystallization models to obtain a comprehensive idea about the microstructure evolution during the high temperature deformation of austenite microalloyed with niobium.

The model for the strain-induced precipitation of NbC is based upon the following four assumptions:

1. The dislocations are evenly distributed throughout the matrix and form a three-dimensional network. The dislocation nodes (illustrated in Figure 10) provide the heterogeneous nucleation sites for the precipitates. A number of earlier workers have shown that NbC is heterogeneously precipitated on the defects, such as subgrain boundaries or dislocations (1, 35). More recently, this has been observed in a model Iron-30 wt% nickel alloy microalloyed with niobium (46). The advantage of using such a model alloy is that it allows the austenite to be stabilised to room temperature. Consequently, it allows for the direct observation of NbC precipitates, and their spatial distribution around the dislocations generated during the deformation of austenite, without the confusing effects of the additional dislocations induced during transformation. Figure 11 shows a distribution of fine (5 nm diameter) NbC particles precipitated in this iron-30 wt% nickel alloy along a subgrain boundary (46). Dutta et al. (35) have also shown that the assumption of dislocation nodes as nucleation sites provides a reasonably accurate description of the precipitate density in these systems.

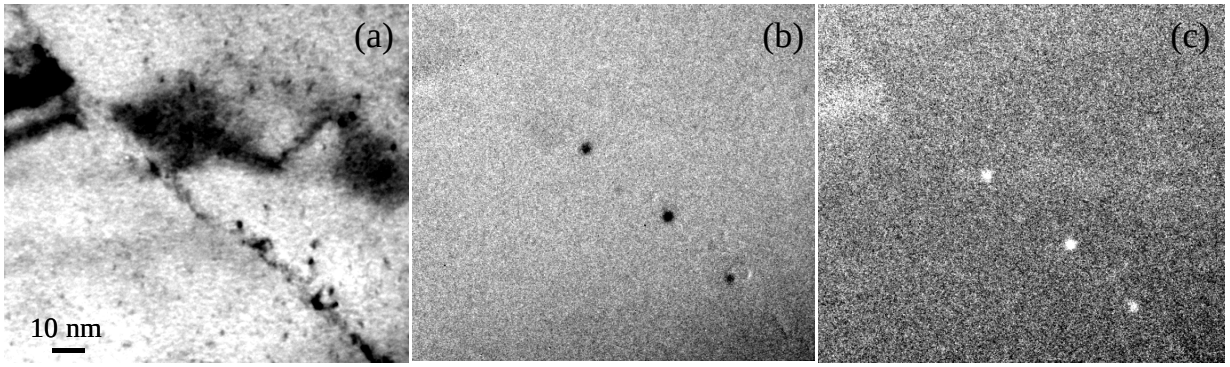

Figure 11: (a) Zero loss filtered bright field image of a subgrain boundary in a Fe-30 wt% Ni alloy prestrained to ε=0.45 at 950ºC at $\dot{\varepsilon}$=10 sec^{-1}, held for 100 seconds, then strained to ε=0.9, followed by quenching to room temperature. (b) Fe M edge jump ratio image. (c) Nb L edge jump ratio image (46).

2. The NbC precipitates are assumed to be spherical, and the critical radius for the nucleation of precipitates on dislocations is the same as that for the general nucleation of precipitates in the bulk. Since the growth and coarsening of the precipitates are very fast on the dislocations, the exact nucleation radius is expected to have negligible influence on the overall precipitation kinetics.

3. The composition of the NbC precipitates is assumed to be stoichiometric and the solubility is calculated using a previously published solubility product, which was derived from direct measurements on a low carbon steel containing 0.02 wt% niobium (38).

4. As the diffusivity of niobium is almost 8-9 orders of magnitude lower than that of either carbon or nitrogen, the diffusion of niobium in austenite has been assumed to be the rate-limiting step for the precipitation process (41, 47).

Nucleation of Precipitation

The activation energy for homogeneous nucleation consists of three parts: (i) the chemical free energy arising from the chemical supersaturation of the solutes, (ii) the interfacial energy spent for creating the precipitate/matrix interface and (iii) the strain energy used to accommodate the strain mismatch. In the present case, the strain energy part is neglected to reduce the complexity. However, as mentioned previously, the present model involves heterogeneous

nucleation with the precipitates being nucleated on the dislocations. The heterogeneous nucleation of incoherent precipitates on dislocations has been studied in detail (48, 49). However, the interaction between the dislocations and the precipitates is very complex in nature. Instead, a simplified assumption is made that the dislocation core energy over the radius of the nucleating precipitates is spent for precipitate nucleation. This hypothesis has been successfully employed previously (28), and it has been shown that the changes in activation energy correspond to the changes in the empirical constants used to describe the precipitation kinetics.

Precipitation is assumed to occur in two stages: (1) in the first stage, precipitates nucleate and grow and (2) in the second stage, when the nucleation ceases, precipitates enter the regime of growth and coarsening. Furthermore, the precipitation on dislocations is assumed to be instantaneous and therefore, the incubation period is assumed to be infinitesimally small. The parameter N_o, which represents the number of available sites for the heterogeneous nucleation, is the number of nodes in the dislocation network and is given as (35):

$$N_o = 0.5 r^{1.5} \tag{3}$$

Where, ρ is the dislocation density at the beginning of precipitation and can be estimated as (35):

$$r = \left(\frac{s - s_y}{M a \mu b} f_r \right)^2 \tag{4}$$

where, σ and σ_y are respectively the flow stress and yield stress at the respective deformation temperature, μ and b represent the shear modulus and Burger's vector, M is the Taylor factor (3.1 for FCC crystals) and α is a constant (=0.15). The constant f_ρ is a 'dislocation density factor' that is used to fit the observed data and predictions. Since the exact value for flow stress is not available for every specific case, this factor is used to adjust the dislocation density.

Growth and Coarsening

As soon as the critical precipitate radius and the mean precipitate radius become nearly equal, coarsening commences (50,51). Since the precipitates are nucleated on dislocations, the coarsening is greatly influenced by pipe diffusion through the dislocation cores. Hence, in the coarsening stage, the bulk diffusion coefficient is replaced by an effective diffusion coefficient which takes care of both the bulk diffusion and the pipe diffusion. The effective diffusivity (D_{eff}) is given by Equation 5:

$$D_{eff} = D_p p R_{core}^2 r + D(1 - p R_{core}^2 r) \tag{5}$$

where, D_p is the pipe diffusion coefficient and R_{core} is the radius of the dislocation core. This effective diffusivity is used for the calculation of the precipitate radius and number density evolution.

Figure 12 shows the evolution of both precipitate number density and volume fraction following single-pass deformation. This behaviour was subsequently compared with the respective number density and volume fraction of NbC precipitates in undeformed austenite. This comparison highlighted the fact that the presence of dislocations provided numerous heterogeneous nucleation sites, and hence, the precipitate number density is approximately four orders of magnitude greater (reaching its maximum value after 3-4 seconds) for the deformed

steel compared with undeformed austenite. In addition, precipitation starts much earlier in the deformed steel, in times almost three orders of magnitude quicker than for undeformed austenite. Coarsening is also much faster in the deformed steel as is evident from the onset of the decrease in the precipitate number density. It is further noted that the precipitate number density in the deformed austenite reaches a maximum very early and subsequently starts decreasing while the precipitate volume fraction is still increasing. This is contrary to the results observed during precipitation in the undeformed austenite, where the precipitate number density reaches a maximum when the precipitation is almost complete (i.e. the precipitate volume percent is nearly 100). This is a result of enhanced coarsening kinetics in the deformed material because of dislocation-assisted diffusion.

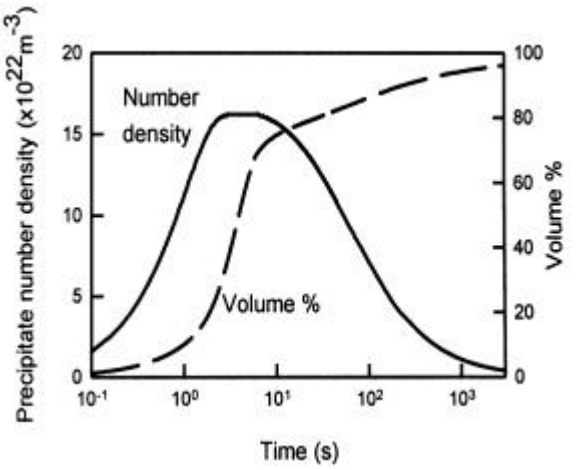

Figure 12: Modelled result showing the effect of prior deformation on the precipitation kinetics in a 0.084C-0.015N-0.06Nb steel, reheated at 1300ºC and subsequently cooled down to 950ºC, deformed at ε=0.33, and held isothermally (40).

Comparison of the Model with Experimental Results

Figure 13 shows a comparison of precipitate size evolution as predicted from the present model with the reported experimental data of Hansen et al. for a steel with a 0.031wt% niobium concentration (33). This steel was reheated to 1250°C for one hour, cooled down to 950°C, followed by a 50% rolling reduction (i.e., an equivalent true strain of 0.8) at a strain rate of $2.6s^{-1}$, and subsequently annealed at various temperatures. A constant deformation temperature and a constant true strain rate signify a constant value of the Zener-Hollomon parameter (Z) for all the conditions. Considering the experimental scatter, it can be concluded that the model shows an excellent agreement with the experimental data (40).

Figure 14 shows the experimentally determined PTT (precipitation-time-temperature) curves (shown as symbols) for a low carbon, low nitrogen steel containing 0.03 wt% niobium as reported by Janampa (41). The present model (40) predictions have also been shown (as lines) in the same plots. In this case, the steels were first given a roughing deformation of 33% (equivalent true strain of 0.46) at 1100°C and then a second deformation of 25% (equivalent true strain of 0.33) at the respective annealing temperatures. Prior to roughing, the steel was austenitised at 1200°C for 45 minutes. It is important to note that the microstructure was completely recrystallised following roughing, which indicates that there was no strain accumulation before the second deformation. A dislocation density factor of 5 was used for the model calculations.

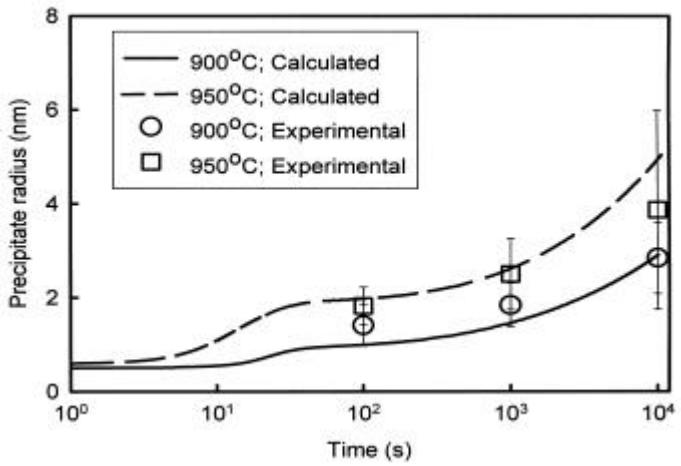

Figure 13: Modelled result [40] showing the variation in precipitate radius with annealing time in steel containing 0.11C-0.01N-0.031Nb-1.35Mn. The reheat temperature was 1250ºC, and the steel was deformed to $\bar{e}$ =0.8 at 950ºC. Experimental data are from Hansen et.al. [33].

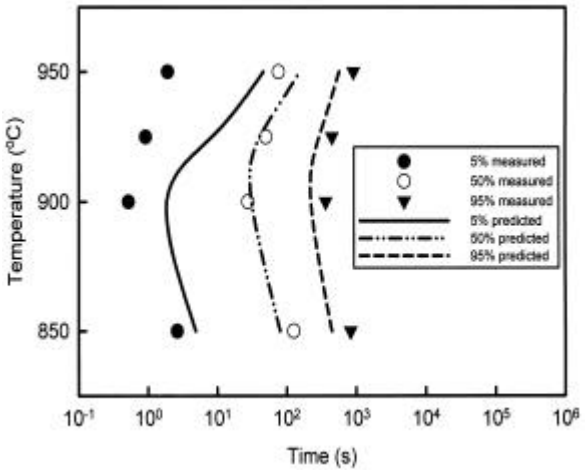

Figure 14: Precipitation-time-temperature plot for a 0.084C-0.006N-0.03Nb steel, reheated to 1250ºC, and deformed to an equivalent true strain of 0.33. Experimental data are from Janampa (41) and are shown as symbols. The modeled results (40) are shown by the lines.

Although the experimental data show an early beginning of the precipitation process (as revealed by 5% precipitation time) compared with the calculated data, the absolute difference between these two is negligible. The discrepancy between the experimental and predicted results is most likely due to the particular experimental technique used for the detection of precipitates. For example, the results from the experimental precipitation studies shown in Figure 13 utilised carbon extraction replicas whereas the experimental results shown in Figure 14 made use of precipitate separation techniques. One important drawback of either of these techniques is the inability to distinguish between the grain boundary precipitation and matrix precipitation, which can lead to an overestimation of the precipitation kinetics. This is the most likely cause for the discrepancy observed in the predicted and experimental values for 5% precipitation shown in Figure 14. This further highlights the importance of high resolution electron microscopy on thin foils of model alloys such as Fe-30wt%Ni (46). Considering the scatters involved in the experiments and holding times before deformation etc., the model predictions are found to be in very good agreement with the experimental observations. It

should be noted that the shape of the PTT curves and the effects of niobium, carbon and nitrogen concentrations on the PTT curves are successfully predicted by the present model (40).

It is important to note that the success of the present model depends to a great extent on the accuracy of the solubility product used to predict the driving force for the precipitation. As has been discussed previously, there is some uncertainty associated with the solubility product in these steels. Alloying elements, such as manganese and silicon, which do not take part in the precipitation, also affect the solubility product through their interactions with the dissolved solutes. Manganese is reported to have a very pronounced effect on the solubility of niobium and this is clearly manifested by its influence on the kinetics of precipitation (12). Therefore, the present study has used a solubility product that was determined by direct measurements through atom probe analysis (38). Furthermore, this solubility product was measured in steels which had similar compositions to those analyzed in the present study. This ensured the applicability of this particular product in the present case.

Besides the effect of the solubility products, the other parameter that plays a key role in determining the precipitation kinetics is the site density for heterogeneous nucleation. As the present model assumes that the dislocation nodes are the nucleation sites, the dislocation density in the matrix is a crucial factor, but an accurate estimation of the dislocation density is very difficult. Primarily, this is affected by the strain, strain rate, temperature and type of deformation. However, there are a host of other factors which govern the dislocation build-up in the material. These include the material composition, type of deformation etc. In the present case, the dislocation density has been estimated from experimental flow stress data, Equation 4. A parameter called the dislocation density factor (f_ρ) has been used to account for the effect of different experimental conditions on dislocation density. It should be remembered that this factor is purely an empirical factor and is used to adjust the value of dislocation density under different deformation conditions so as to obtain the best fit between the predictions and experimental observations. It is well known that the flow stress is significantly influenced by the deformation conditions (as mentioned before) as well as material parameters, such as bulk material composition, and specifically on the amount of dissolved solute, grain size etc. All of these factors that affect the flow stress (and thereby the dislocation density) are expected to influence the value of the dislocation density factor. In addition to this, the prior history of the material also plays an important role (this has been observed by various workers (28)). A finer matrix grain size, obtained by a high temperature roughing deformation and recrystallization is found to enhance the precipitation kinetics significantly. This has been attributed to a 'conditioning effect' of the matrix caused by the roughing deformation and following recrystallization, and some grain boundary precipitation (28).

In the present model, the effect of pipe diffusion along dislocations is accounted by using an effective diffusion coefficient (Equation 5) instead of the bulk diffusion coefficient during the coarsening of precipitates. It is known that the diffusion process can be well represented by an effective diffusion coefficient when the lattice diffusional length, $(D_l t)^{1/2}$ is significantly greater than the spacing (l) between the short-circuit paths (52). In the present study, this criterion is found to be valid in all the cases. For an example, in Figure 10, the spacing between the short circuit paths (i.e. the distance between the dislocation nodes) was found to be almost half of the diffusional length at the onset of coarsening. As the precipitation proceeds, the diffusional length increases further with increasing annealing time and the use of an effective diffusion coefficient becomes more and more appropriate.

In summary, it can be noted that the present model (40) for the strain-induced precipitation of NbC provides a complete evaluation of the precipitation kinetics and hence, can be used to calculate both of the above mentioned temperatures in conjunction with a model predicting the

kinetics of recrystallization. In particular, the estimation of the precipitate pinning force requires a prior knowledge of precipitate size and volume fraction. To date, most of the researchers who tried to estimate the pinning force have used equilibrium precipitate volume fraction as an input parameter. A quick look at typical delay times in between successive deformation steps during practical operations reveals that the time periods are short and precipitate volume fraction does not reach the equilibrium value in this short time. Hence, calculations using equilibrium precipitate volume fraction will lead to an overestimation of the magnitude of the pinning force. The present model will help to obtain an accurate value of precipitate volume fraction. Furthermore, the time evolution of pinning force can also be obtained from the knowledge of the precipitate size and volume fraction evolution using the present model (40). It is important to note, however, that the present model is based on the underlying physics associated with single-pass deformation, which clearly makes it an inadequate model for multi-pass deformation, to be discussed in the next section. Nevertheless, the power of the present model rests with it representing a fundamental building block for subsequent multi-pass deformation models.

Industrial Rolling Applications

All industrial rolling of flat products from conventional slab involves multiple passes carried out over a temperature range which varies widely for plate, strip rolled on tandem mills and strip rolled on steckel mills. The processing is divided into the roughing stage, which is broadly similar for the three product routes, and the finishing stage which is very different for each route.

Rough Rolling

As discussed earlier, reheating aims to maximize the amount of the microalloying element taken into solution and to homogenize the solute concentration in the austenite matrix. It is never fully effective, but the consequence of holding the steel at a high temperature for long times is to coarsen the austenite grains. The metallurgical objective of the roughing passes is therefore to refine the grains by repeated recrystallization between passes. This means that roughing should be complete before the temperature falls to the recrystallization-limit ($T_{95\%}$) temperature, because partial recrystallization leads to a mixed grain structure which cannot be eliminated by subsequent finishing passes when the temperature falls below the recrystallization-stop ($T_{5\%}$) temperature. The simple model (28) is reasonably successful in predicting the effects of composition and process variables on the grain size evolution in roughing, but experimental observations indicate that more attention must be paid to the further development of the model to take into account: First, the occurrence of relatively coarse precipitation of Nb(C,N), which has little effect on recrystallization, but drains the microalloying elements from solution, so that they are not available for transformation hardening. In simple niobium steels, the loss of solute probably arises from grain boundary nucleation or growth of undissolved coarse particles, particularly in regions of residual segregation (53). In niobium-titanium steels, the finer TiN particles remaining after reheating can act in a similar way, and if a small enough interparticle spacing can be generated, the epitaxial growth of NbC can lead to the retardation of recrystallization and a major increase in $T_{95\%}$ (27). A second effect of roughing passes in accelerating the kinetics of strain-induced precipitation in finish rolling has been observed (54,55) and attributed to equilibrium microsegregation or clustering of the niobium. It is also possible that non-equilibrium clustering due to the elimination of excess vacancies between passes plays a significant role (56). While these effects can be allowed for empirically, today's models of roughing do not consider the phenomena in the basic sense that is necessary if the state and distribution of

microalloy elements in solution is to be passed on to the precipitation models applied to finish rolling.

Finish Rolling

The temperature time histories during the finishing of plate and of strip by tandem mill and steckel mill rolling of strip are so different in relation to both the recrystallization and precipitation start curves that they will be considered separately.

Plate Rolling. Early modelling of controlled rolling established that the recrystallization-stop temperature is determined by sufficient strain-induced precipitation occurring before the onset of recrystallization to provide pinning and prevent the nucleation of recrystallization. For conventional controlled rolling of plate, the start finishing temperature is below the recrystallization-stop temperature, and strain accumulation takes place throughout the finish rolling process.

The recent model (40) discussed earlier for the kinetics of strain-induced precipitation and coarsening after a single rolling pass based on Figures 10a and 10b indicates that for industrial plate rolling conditions, only a small volume fraction of precipitation will have occurred before the second finish rolling pass. The deformation in the second pass will cause a change in the arrangement of the dislocation network, with the consequences illustrated schematically in Figure 15 (35). As shown in Figure 15a, many dislocation nodes will be displaced from the positions at which particles are nucleated after the first finishing pass. This has two important consequences: First, the rapid pipe diffusion paths for particle coarsening are removed, so the coarsening rate, and hence the rate of reduction of particle number density will be dramatically reduced. Second, the majority of the new dislocation nodes will lie in volumes of the matrix in which the solute content has not been depleted by growth of the precipitates after the first pass. Additional nucleation of new particles should therefore occur (Figure 15b) to increase the number density of the precipitates. Direct evidence for this is provided by the experimental observations shown in Figure 16, in which incremental hardening above that expected for the cumulative strain hardening is observed for sequential finishing passes at equivalent temperatures (57). This increased pinning ensures that no recrystallization takes place during finishing rolling, despite the increase in stored energy. It also results in an increase in total volume fraction of precipitates, and consequently a reduction in the residual microalloy content in solution to provide transformation hardening.

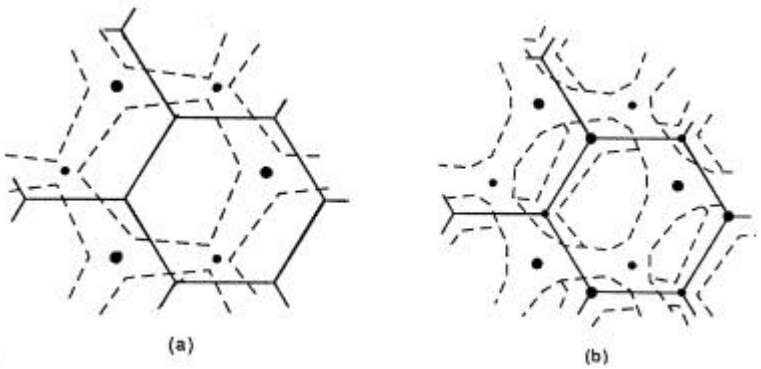

Figure 15: Schematic diagram of the dislocation and particle distribution created (a) by a second finishing deformation and (b) by holding after a second finishing deformation. Solid lines represent dislocations and dashed lines indicate the limits of the solute depleted regions (35).

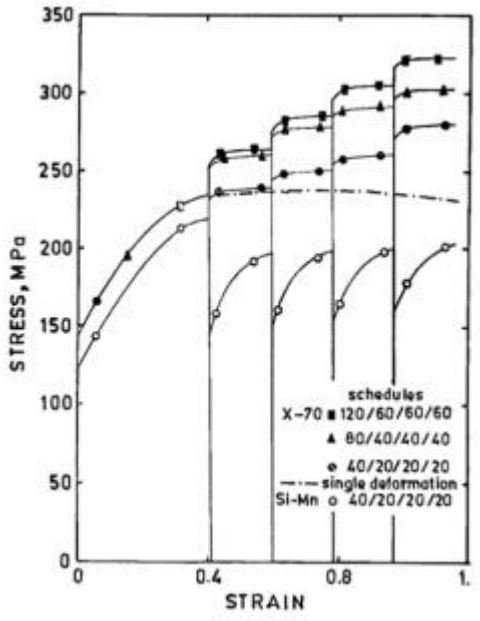

Figure 16: Stress-strain curves at 850°C and a strain rate of $5s^{-1}$ for reduction schedules of 30/15/15/15/15% with various time intervals between deformations for Si-Mn and X70 plate steels (57).

Currently, these modelling concepts are not yet quantitative, but the model (40) presented for the kinetics of precipitation after a single rolling pass provides an important and fundamental base for the development of a model for precipitation during multi-pass finishing, which can be validated by experimental observations of the change in flow stress in sequential passes. This is clearly an important step in providing information about the solute content and its spatial distribution for modelling transformation and precipitation during air cooling or accelerated cooling of plate after finish rolling.

Strip Rolling. During conventional rolling of strip in a 6 or 7 stand tandem mill, the strain rates increase progressively from ~20 s^{-1} to ~200 s^{-1}, and the time intervals between passes decrease from ~2 s to ~0.2 s during finish rolling.

Currently, there is an enigma about the mechanisms controlling microstructural evolution, because the high strain rates and short interpass times preclude direct simulation of finish rolling in laboratory tests (58, 59). Torsion testing at lower strain rates of 2 s^{-1} (60) indicates that no strain-induced intragranular precipitation occurs in the short interpass times and that partial softening takes place by metadynamic recrystallization following dynamic recrystallization during the finishing passes, as a result of strain accumulation (61). There is evidence of partial softening between passes during industrial rolling (58), but it is not clear whether dynamic recrystallization can take place during passes at the high strain rates of industrial rolling (59). Partial softening could arise from partial static recrystallization at high accumulated strains, but the present models do not enable one to decide between the alternative mechanisms. Further development of the models is therefore important, because it is unlikely that developments in laboratory simulation methods alone can progress the current physical understanding to the high strain rates of industrial strip processing.

Steckel Mill Rolling. Steckel rolling mills have the potential to change the economics of the flat rolled steel production worldwide, mainly because of lower capital costs and the flexibility in production quantities. The interpass time in steckel mill rolling is rather long, ranging from

30–100 seconds in comparison with 0.2-2 seconds in a semi-continuous multi-stand rolling mill. This leads to a substantial difference in the finish rolling caused by static softening in the long interpass times in steckel rolling. Modelling results, laboratory studies and mill trials have confirmed the distinct advantage of a high niobium (>0.08wt%) low interstitial (<0.03wt%carbon and <0.003wt%nitrogen) design in the development of high-strength high-toughness plates for line pipe application using steckel mill rolling.

The strategy for steckel mill rolling of high niobium low interstitial steel consists of lowering the temperature of finish rolling to well below the nose of the precipitation-time-temperature (PTT) curve for strain-induced precipitation of NbC. A low nitrogen design with a titanium addition to the stoichiometric requirement to tie up all the nitrogen at high temperature as TiN allows all of the niobium to be in solution in austenite, which retards the static recrystallization in the low temperature window before the onset of the strain-induced precipitation of NbC. The pinning pressure due to the strain-induced precipitation of NbC is more effective than solute niobium in retarding the static recrystallization in the inter-pass time. Nucleation and growth of the precipitates occurs in a similar way to that described earlier for plate finishing. Thus, strain accumulation in finish rolling is aided by giving an adequate number of large reductions so that the pinning pressure is increased through increasing the number of particles progressively through nucleation rather than decreasing the number of particles by coarsening. However, a residual niobium of 0.04 wt % in the matrix is required in order to obtain additional strengthening due transformation hardening and precipitation strengthening upon transformation (62, 63). Therefore it is essential to restrict the number of passes so that the precipitates deplete only a fraction (about 50 %) of the total niobium in the matrix. The low temperature window decreases the diffusion kinetics so that the residual solute niobium in the matrix is adequately high. Typically, the temperature window for finish rolling for a high niobium (>0.08wt%) steel is in the range of 850-730ºC, the pass reduction typically in the range of 30-15% and the number of passes is five or less for a grade 80 line pipe steel.

Concluding Remarks

This paper has considered the state-of-the art of modelling of thermomechanical rolling from casting to the end of the rolling process. For a complete through-process model, this is only the input required for a transformation model of the microstructure developed on cooling, which in itself is the input for properties and attributes models. It may seem that the complexities already encountered make development of true through-process models a serious challenge. However, first of all one can recognize the advances that have been made since Niobium 1981 and second, one can see that the concept of through-process modelling has revealed which parts of the process have been modelled with a considerable degree of sophistication and which parts have been overlooked.

For an effective through-process model, every step should have inputs and outputs that progress the model at a consistent level. The experimental back-up necessary to make this feasible can therefore be built into future research strategy. This inevitably leads the authors to the view that enough relevant experiments to cover all the process variables cannot be carried out in laboratories on a realistic time scale for a complete physically based, or “white box” model to be developed. The developments that have taken place in alternative modelling paradigms, such as neural networks and genetic algorithms, for analysing and optimizing process variables from data recorded by sensors in industrial processing must therefore be recognized. These provide an efficient means of “black box” modelling for control of specific plant or processes, because with appropriate training sets of data, they enable rapid computation of the control variables in the later stages of processing, which are required to compensate for compositional

or processing variations in the earlier stages of processing. Such models are, however, only valid within the window of data on which they are based.

It is now possible to combine the "white-box" and "black-box" methodologies to develop "grey-box" modelling for example as illustrated in Figure 17 (64). Here, the best available physically-based model (i.e, some prior model) provides the foundation, but the wealth of industrial data (i.e., neural networks) provides a refinement of the quantitative predictions within the narrow range of variables, which produce acceptable quality of products on a particular plant.

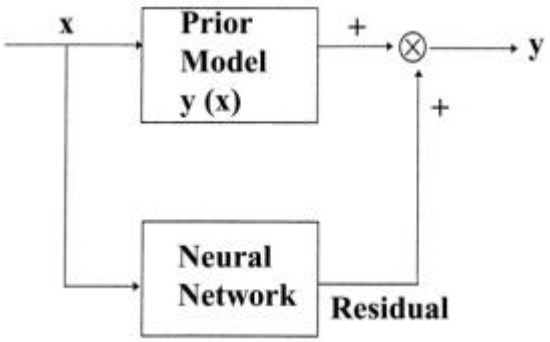

Figure 17: Schematic flow chart illustrating grey-box modelling from both black and white-box methodologies (64).

Before "Niobium 2021", this combined modelling methodology, undertaken by multidisciplinary teams, with individual expertise in each of the specialist areas involved, does offer the prospect of truly "through-process" models, which incorporate the best scientific base available and the wealth of industrial know-how. These models can then encapsulate the "corporate wisdom", which was traditionally developed through long term stability of employment from apprentice to senior technical manager. Today, "lean" companies with employee mobility have already lost this route to advancing corporate wisdom, so the development of comprehensive through-process models is a socially, as well as a technically driven requirement, for continued future competitiveness.

References

(1) A.J. DeArdo, J.M. Gray and L. Meyer, Niobium 81 (San Francisco), Ed. H. Stuart, (Warrendale, PA: TMS-AIME, 1984), 685.

(2) C.M. Sellars and J.A. Whiteman, Controlled Processing of High Strength Low Alloy Steels (York), (Sheffield, UK: British Steel Corporation, 1976).

(3) C.M. Sellars, Hot Working and Forming Processes (Sheffield), eds. C.M. Sellars and G.J. Davies, (London, UK: The Metals Society, 1980), 3.

(4) J.H. Beynon and C.M. Sellars, Modelling of Plastic Deformation and its Engineering Applications, eds. S.I. Andersen et.al., (Denmark: RISθ National Laboratory, 1992), 13.

(5) Y.H. Li et.al., Acta Metallurgica Sinica (English Letters), 13 (2000), 359.

(6) J. Andorfer et.al., Thermec 97 (Wollongong), eds. T. Chandra and T. Saki, (Warrendale, PA: TMS-AIME, 1997), 2069.

(7) D.C.Houghton, G.C.Weatherly and J.D.Embury, Advances in the Physical Metallurgy and Applications of Steels, (New York, NY: TMS-AIME, 1982), 267.

(8) M.Hillert and L.I.Staffansson, Acta Chemica Scandinavica, 24 (1970), 3618.

(9) K.J.Irving, F.B.Pickering and T.Gladman, J. Iron and Steel Inst., 205 (1976), 161.

(10) H.Ohtani et al., Japan-Canada Seminar on Secondary Steelmaking, 3-4 December, 1985, J7.

(11) S.Koyama, T.Ishii and K.Narita, Nippon Kink, Gakk, Vol. 35 (1971), 1089.

(12) M.G.Akben, I.Weiss and J. J. Jonas, Acta Metall., 29 (1981), 111.

(13) K.Balasubramanian and J.S.Kirkaldy, CALPHAD, 10 (1986), 187.

(14) J.M.Gray, S.V.Subramanian and D.A.R. Kay, Technology and Applications of HSLA Steels (Philadelphia), (Metals Park: ASM, 1983), 967.

(15) T.Nishizawa, The 131st and 132nd Nishiyama Memorial Seminar, Prediction of Control Technology of the Mechanical Properties of Steel: Present and Future Status, (Tokyo: ISIJ, 1990), 17.

(16) S.Akamatsu et al., ISIJ International, 24 (1994), 9.

(17) K.Inoue et al., ISIJ International, 41 (2001), 175.

(18) E.Rudy, J. of the Less-Common Metals, 33 (1970), 43.

(19) M.Grujicic, I.Wang and W.S.Owen, CALPHAD, 10 (1986), 117.

(20) H.Zou and J.S.Kirkaldy, Metall. Trans., 23 (1992), 651.

(21) M.Prikryl et al., Metall. Trans., 27 (1996), 1149.

(22) H.G.Suzuki, S.Nishimura and S.Yamaguchi, Trans. Iron Steel Inst. Japan, 22 (1982), 48.

(23) C.Ouchi and K.Matsumoto, Trans. Iron Steel Inst. Japan, 22 (1982), 181.

(24) Y.Maechara and Y.Ohmori, Mat. Sci. Eng., 62 (1984), 109.

(25) S.V.Subramanian et al., Technology and Applications of HSLA Steels (Beijing), (Materials Park: ASM International, 1985), 151.

(26) T.Taira et al., Technology and Applications of HSLA Steels (Philadelphia), (Metals Park: ASM, 1983), 723.

(27) S.V.Subramanian et al. Microalloyed Bar and Forging Steels (Hamilton), ed. M. Finn, (Montreal: CIM, 1990), 120.

(28) B.Dutta, and C.M.Sellars, Mat. Sci. Tech., 3 (1987), 197.

(29) S.V.Subramanian and G.C.Weatherly, Thermec 97 (Wollongong), eds. T. Chandra and T. Saki, (Warrendale, PA: TMS-AIME, 1997), 827.

(30) S.V.Subramanian and H. Zou, Processing, Microstructure and Properties of Microalloyed and Other Modern High Strength Low Alloy Steels (Pittsburgh), (Warrendale: ISS-AIME, 1991), p. 23.

(31) D.R.Poirier et al., J. Iron and Steel Inst., 199 (1970), 371.

(32) D.H. Geiger and D.R. Poirier, Transport Phenomena in Metallurgy, (Reading, MA: Addison-Wesley Publishing Co., 1973), 497.

(33) S.S. Hansen, J.B. Vander Sande, and M. Cohen, Metall. Trans., 11 (1980), 387.

(34) W.J. Liu and J.J. Jonas, Metall. Trans., 20 (1989), 689.

(35) B. Dutta, E. Valdes and C.M. Sellars, Acta Metall. Mater., 40 (1992), 653.

(36) E.J. Palmiere, C.I. Garcia, and A.J. DeArdo, Metall. Trans., 27 (1996), 951.

(37) B. Dutta and E.J. Palmiere, Metall. Mater. Trans., In press, 2001.

(38) E.J. Palmiere, C.I. Garcia and A.J. DeArdo, Metall. Mater. Trans., 25 (994), 277.

(39) W.J. Liu, Metall. Mater. Trans., 26 (1995), 1641.

(40) B. Dutta, E.J. Palmiere and C.M. Sellars, Acta Mater., 49 (2001), 785.

(41) C.S. Janampa, Ph.D. thesis, The University of Sheffield, 1982.

(42) C.M. Sellars, Mat. Sci. Tech., 6 (1990), 1072.

(43) K.C. Russell, Adv. Coll. Int. Sci., 13 (1980), 205.

(44) R. Wagner, R., and R. Kampmann, R. in: Mater. Sci. Tech. A Comprehensive Treatment, eds. R.W. Cahn, P. Hassen and E.J. Krammer, Vol. 5, (VCH Verlagsgesselschaft GmbH, Weinheim, Germany, 1991), 213.

(45) K.C. Russell, in: Phase Transformations, eds. H.I. Aaronson, (Metals Park: ASM, 1970), 219.

(46) M.P. Black et.al., Acta Mater., In press, 2001.

(47) S. Kurokawa, J.E. Ruzzante, A.M. Hey, and F. Dyment, Metals Sci., 17 (1983), 433.

(48) J.W. Cahn, Acta Metall., 5 (1957), 169.

(49) R. Gomez-Ramirez, and G.M. Pound, Metall. Trans., 4 (1973), 1563.

(50) I.M. Lifshitz, and V.V. Slyozov, J. Phys. Chem. Solids, 19 (1961), 35.

(51) C. Wagner, Z. Electrochem., 65 (1961), 581.

(52) G.A. Murch, in: Mater. Sci. Tech. A Comprehensive Treatment, eds. R.W. Cahn, P. Hassen and E.J. Krammer, Vol. 5, (VCH Verlagsgesselschaft GmbH, Weinheim, Germany, 1991), 90.

(53) D.R. DiMicco and A.T. Davenport, Thermomechanical Processing of Microalloyed Austenite (Pittsburgh), eds. A.J. DeArdo, G.A. Ratz and P.J. Wray, (Warrendale: TMS-AIME, 1982), 59.

(54) E. Valdes and C.M. Sellars, Mat. Sci. and Tech., 7 (1991), 622.

(55) E.S. Siradj, C.M. Sellars and J.A. Whiteman, Mat. Sci. Forum, 284-286 (1998), 143.

(56) M. Militzer and D. Meade, Thermomechanical Processing of Steel (Ottawa), eds. S. Yue and E. Essadiqi, (Montreal: CIM, 2000), 453.

(57) B. Dutta and C.M. Sellars, Thermec 88 (Tokyo), Ed. I. Tamura, (Tokyo: ISIJ, 1988), 261.

(58) J.J. Jonas, Thermec 97 (Wollongong), eds. T. Chandra and T. Saki, (Warrendale, PA: TMS-AIME, 1997), 31.

(59) C.M. Sellars, Thermomechanical Processing of Steel (Ottawa), eds. S. Yue and E. Essadiqi, (Montreal: CIM, 2000), 3.

(60) L.N. Pussegoda, S. Yue and J.J. Jonas, Metall. Trans., 21 (1990), 153.

(61) C. Roucoules, S. Yue and J.J. Jonas, Modelling of Hot Rolling Processes (London), (London: The Institute of Materials, 1993), 165.

(62) S.V. Subramanian et. al., Low Carbon Steels for the 90's (Pittsburgh), eds. R. Asfahani and G. Tither, (Warrendale: TMS-AIME, 1993), 313.

(63) L.E. Collins et.al., Microalloying 95 (Pittsburgh), ed. M. Korchynsky, (Warrendale: ISS-AIME, 1995), 141.

(64) D.A. Linkens, J.H. Beynon and C.M. Sellars, Australia Pacific Forum on Intelligent Processing and Manufacturing of Materials, eds. T. Chandra et.al., Vol. 2, (Australia Pacific Forum, 1997), 676.